Competition between nucleation and confinement in the crystallization of poly(ethylene glycol)/ large aspect ratio hectorite nanocomposites

Christoph Habel[1,†] Jon Maiz[2,†], Jorge L. Olmedo-Martínez[2], Juan V. López[3], Josef Breu[1], Alejandro J. Müller[2,4*]*

[1] Bavarian Polymer Institute and Department of Chemistry, University of Bayreuth, Universitätsstraße 30, Bayreuth, 95447, Germany

[2] POLYMAT and Polymer Science and Technology Department, Faculty of Chemistry, University of the Basque Country UPV/EHU, Paseo Manuel de Lardizábal 3, 20018 Donostia-San Sebastián, Spain

[3] USB Polymer Group, Department of Materials Science, University Simón Bolívar, Apartado 89000, Caracas 1080-A, Venezuela

[4] IKERBASQUE, Basque Foundation for Science, Bilbao, Spain

† These authors contributed equally to this work.

*Corresponding Authors

E-Mail address: alejandrojesus.muller@ehu.es, Tel: +34 943018191

josef.breu@uni-bayreuth.de, Tel: +49 921552531

ABSTRACT

The overall crystallization kinetics of polymer nanocomposites is determined by nucleation and crystal growth, which are both greatly affected by confinement. Heterogeneous nucleation is influenced by the interphase area between filler and polymer matrix. Starting with a homogeneous nematic aqueous dispersion of a mixture containing polyethylene glycol (PEG) and varying amounts of a high aspect ratio layered silicate (hectorite, Hec), nanocomposite films were casted displaying a systematic variation of the degree of PEG confinement. This is achieved by a partial phase segregation upon drying, where independently of filler content a thermodynamically stable, 1 dimensional crystalline hybrid with constant volume of intercalated PEG (0.81 nm corresponding to a fraction 75 wt% and 55 vol%, respectively) is formed. This intercalated hybrid phase is incorporated into segregated PEG domains. The segregation is a kinetically controlled process and the length scale of segregation increases with PEG available in surplus of the hybrid. Due to the very large lateral extension of the Hec, the segregated domains are increasingly two dimensional. As evidenced by transmission electron micrographs and powder X-ray diffraction, the segregation produces composite structures where, in dependency of filler content, PEG slabs of different thickness are separated by domains of the intercalated hybrid material. The crystallization behavior of these bi-phasic materials was investigated by Differential Scanning Calorimetry (DSC) and Polarized Light Optical Microscopy (PLOM). DSC results reveal a competition between the nucleating effect of Hec, which was particularly important at low amounts, and the PEG confinement effect at higher filler loadings. Applying a self-nucleation protocol, the nucleation efficiency of the hectorite was shown to be up to 67%. The isothermal crystallization kinetics accelerated at low Hec contents (nucleation), went through a maximum and then decreased (confinement) as Hec content increased. Additionaly, a clear correlation between filler content and the Avrami index was obtained supporting the increase in confinement as filler loading increased.

Keywords: Hectorite/PEG nanocomposites, Nucleation, Confinement

1. Introduction

Polymeric nanocomposites are remarkable materials, because of their morphology and properties and the large variety of existing nanofillers.[1-3] Furthermore, these nanofillers can improve many properties of the matrix, such as mechanical, fire retardancy, barrier quality, thermal resistance and conductivity. When the nanofiller content increases beyond a percolation threshold, normally, confinement effects can develop.[4]

Polymers can be confined in one dimension (ultra-thin films, nanolayers, nanoscopic phases within block copolymers), two dimensions (nanocylinders in AAO templates or strongly segregated block copolymers) or three dimensions (3D micro or nano domains within blends, block copolymers, etc.).[5] The behavior of polymers in restricted space can be dramatically different than in bulk[6], in particular when nanodomains reach sizes comparable to the radius of gyration of the chains. Thermal transitions in confined polymers change according to the level of confinement, as well as crystal orientation.

Nucleation and crystallization depend on the size and number of crystallizable domains or microdomains. When the number of micro or nanodomains is similar to the number of heterogeneities present in a bulk polymer, the crystallization of the confined material can be divided into several exotherms upon cooling from the melt at distinct supercoolings in a process know as fractionated crystallization. The different crystallization peaks are due to the different populations of confined microdomains that have different nucleation mechanisms. Typically the nucleation changes from heterogeneous at high temperatures (where one or more exotherms can correspond to heterogeneities that have different activation energies) to surface or homogeneous nucleation at very high supercoolings, close to vitrification, as the degree of

confinement increases or the size of the microdomain decrease. If the number of microdomains is several orders of magnitude higher than the number of available heterogeneities in the bulk material, the crystallization occurs in a single crystallization peak that corresponds to surface or homogeneous nucleation.[4]

Polyethylene oxide (PEO) and its low lower molecular weight equivalent, know as polyethylene glycol (PEG), are known to be water-soluble and non-ionic polymers of great interest in several fields of application. Beside their use as drug delivery systems, they are mainly used as hydrogels, wound healing materials, tissue engineering and in the field of cell culture.[7-10] Moreover, they have been studied in confined systems, for example with carbon nanotubes (CNT), with silica, in block copolymers and blends.[11, 12] In the case of polymer-filler systems, for example, polyethylene oxide (PEO), polyethylene (PE) and polycaprolactone (PCL) with carbon nanotubes, the effect of the concentration of the filler on the crystallization of the polymer has been studied. At low concentrations the filler can act as a nucleating agent, whereas at high concentrations a confinement effect may occur.[13]

Recently, Wen *et al.*, studied the confined crystallization of methoxypolyethylene glycol (MPEG) grafted to silica as a function of grafting density and molecular weight. They showed that confinement is stronger for lower molecular weight grafted MPEG. Their results demonstrated how the crystallization temperature (T_c) and the crystallinity of grafted MPEG chains reduces with decreases in grafting density. They also fitted their results to the Avrami equation and found that the Avrami index had a value of n ≈ 3 for neat MPEG as the material formed instantaneous spherulites. Instead, for MPEG-g-SiO_2, the Avrami index was less than 1 (at high silica loadings). This result showed that the overall crystallization kinetics was dominated by nucleation, a typical result of confined crystallization.[14]

The main objective of this work is to study the nucleation and confinement effect of a layered silicate with high aspect ratio on PEG in dependancy of the filler content. The used silicate polymer dispersions and the resulting composites are characterized via Small Angle X-Ray Scattering (SAXS) and X-Ray Diffraction (XRD) techniques, respectively. Furthermore, the influence of the resulting structures on the crystallization kinetics of PEG is investigated by DSC measurements. Additionally, the nucleating efficiency of the synthesized layered silicate on PEG were estimated by self-nucleation studies and confirmed by polarized light optical microscopy (PLOM). A potential application for these materials could be food packaging, as low molecular PEG is known to be biocompatible and biodegradable.[15]

2. Experimental Section

2.1 Materials and samples preparation

Sodium hectorite $[Na_{0.5}]^{inter}[Mg_{2.5}Li_{0.5}]^{oct}[Si_4]^{tet}O_{10}F_2$ (Hec) was prepared emploting a synthesis procedure from the melt, previously reported in the literature.[16, 17] The material features a cation exchange capacity (CEC) of 1.27 mmol g^{-1}. Polyethylene glycol (PEG, Mw = 1450 g mol^{-1}) was provided by Sigma Aldrich (Germany). Hec was immersed into Millipore water (1 wt%) for its delamination, and this suspension was added dropwise during stirring to a 1-5 wt% PEG solution in the weight ratios (wt%) PEG:Hec 80:20, 60:40, 40:60 and 25:75 and shaken overnight to improve dispersion quality. Afterwards, the dispersions were cast into Teflon containers and dried (room temperature and 40°C for 7 days (under vacuum), 10^{-3} bar). The different samples are labeled as PEGHec-X with X describing the filler content of Hec in wt%. For comparison, a neat PEG sample was used.

2.2 Characterization

Structural Characterization. PEGHec composites were thinly cut with an Ion Slicer EM-09100IS (JEOL GmbH, Germany), which were then observed with a JEM-2200 FS (JEOL GmbH, Germany transmission electron microscope (TEM).

The diameter of the Hec platelets were measured via scanning electron microscopy (SEM, Zeiss Leo 1530).

A small-angle X-ray "Ganesha AIR" (SAXSLAB, Denmark) equipment was used to record SAXS patterns. It is equipped with a rotating anode X-ray source (copper, MicoMax 007HF, Rigaku Corporation, Japan). A position-sensitive detector (PILATUS 300K, Dectris) was employed to record the diffraction patterns. Prior to the measurements, the PEGHec suspension was centrifuged for 2 hours (13000 rpm) to a resulting gel (4.5 wt%) to enhance sensitivity. The measurement of the suspension was performed in 1 mm glass capillaries (Hilgenberg, Germany) at room temperature. The birefringence of the dispersions was shown with a self-made cross polarizer.

Wide angle X-ray diffraction (XRD) patterns were measured using nickel filtered Cu-K_α radiation (λ = 1.54187 Å) with a Bragg-Brentano-type diffractometer (Empyrean) equipped with a Pixcel detector. The dispersions were dropped onto glass platelets and dried for 1 week in a vacuum chamber (10^{-3} bar). The X-ray diffraction powder patterns were analyzed with a software by Panalytical's Highscore Plus.

The semi-crystalline morphology of neat PEG and PEGHec nanocomposites were examined with polarized light optical microscopy (PLOM) with an OLYMPUS BX51 microscope equipped with an OLYMPUS SC50 camera and a hot-stage (Mettler FP82HT) with liquid nitrogen flow. Samples were prepared by heating them in between glass slides to a temperature of 30 ºC above their melting temperatures to erase thermal crystalline history. After 5 min at this temperature, the samples were cooled at 50 ºC min^{-1} until the desired isothermal T_c value, which was selected based on prior DSC measurements.

Thermal Analysis. A PerkinElmer 8000 DSC equipment with a cooling accessory (an Intracooler II) was used. Ultrapure nitrogen was used as purge gas, and calibration with indium and tin standards was performed. Sample weight was approximately 5 mg. Non-isothermal scans were performed after melting for 3 min at 80 ºC to erase thermal history. Employing scanning rates of 20 °C $min^{-1,}$ a cooling scan from the melt was recorded (down to 0 ºC) followed by a subsequent heating scan (from 0 ºC to the 80 ºC).

We followed the procedure recommended by Lorenzo et al.[18] to measure by DSC experiments, the overall isothermal crystallization rate of the samples, which includes primary nucleation and growth processes. The samples were heated to 80 °C and kept at this temperature for 3 min. Then the samples were rapidly cooled at 60 °C min^{-1} to the isothermal crystallization temperature (T_c). The T_c range employed was previously determined by ensuring that no crystallization occurred during the cooling step. In this way, the minimum isothermal T_c value was chosen when the subsequent heating step showed no melting peak.[18]

Self-Nucleation (SN) was performed according to the protocol of Fillon et al..[19] In this test, the following steps are carried out at 20 ºC min^{-1}: (i) heating the sample to 80 ºC and keeping at this temperature for 1 min to erase thermal history; (ii) the sample is then cooled from 80 ºC to 0 ºC; (iii) heating to a temperature that is denoted self-nucleation temperature (T_s), and the sample remains at this T_s temperature for 5 min; (iv) cooling from T_s to 0 ºC to record any changes in T_c due to SN; and (v) a final heating scan is performed from 0 °C to 80 °C. There are three different SN *Domains* that are well-defined in the literature[19, 20], and will be explained in the results and discussion section below.

3. Results and discussion

Melt synthesized sodium fluorohectorite ($[Na_{0.5}]^{inter}[Mg_{2.5}Li_{0.5}]^{oct}[Si_4]^{tet}O_{10}F_2$, Hec)[16] comes in high lateral dimensions (20 µm) and shows the rare phenomenon of osmotic swelling delivering ≈ 1 nm thick nanosheets of huge aspect ratio (≈ 20 000). The latter renders it ideally suited as filler for poymer composite barriers as needed e.g. in (food) packaging.[21-23] By immersing Hec into deionized water osmotic swelling allows for complete and gentle delamination.[16, 24, 25] As Hec has a very large aspect ratio, the rotation of the nanosheets is stalled and instead of isotropic suspensions, rather liquid crystalline, nematic pahses are obtained. The separation of adjacent nanosheets is well defined and determined by its concentration.[26]

Mixing the nematic Hec dispersion with different amounts of an aqueous PEG solution, allows the polymer to uniformally diffuse between adjacent Hec nanosheets yielding perfectly homogeneous ternary nematic dispersions, as evidenced by SAXS (**Figure 1**). For instance for one of the dispersions (PEGHec-75), a nematic suspension was obtained with 42 nm separation of the nanosheets. Reaggregation of

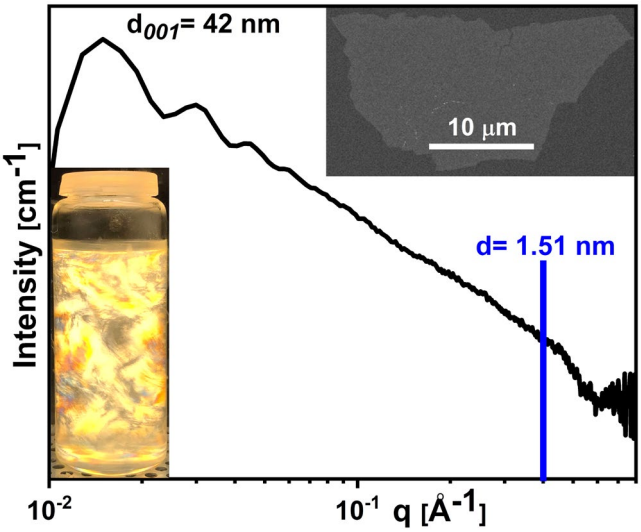

Figure 1. SAXS pattern of the ternary dispersion (PEG, Hec (75 wt%), water) showing completely separated single nanosheets without any reaggregation of the Hec nanosheets evidenced by absence of a reflection at d=1.51 nm (blue line). The insets show a SEM picture of a Hec platelet exhibiting an lateral dimension of > 20 µm and the birefringence of the PEGHec-20 hybrid in a self-made cross polarizer.

Hec nanosheets to stacks can be excluded by the absence of a reflection typical for crystalline hydrated Hec phases at q = 0.65-0.41 $Å^{-1}$ (1.51 nm, indicated as blue line in Figure 1).[16, 26]

These suspensions were cast into Teflon shells and then slowly but thoroughly dried whereupon self-standing films with Hec contents varying from 20 to 75 wt% were obtained. Regardless of the filler content, for all composites a d_{001} peak at 1.77 nm (2θ = 4.97°) was observed by XRD (**Figure 2**). The highly rational *(00l)*-series with sharp and intense basal reflections visible up to the sixth order indicate a well defined 1 dimensional (1D) order.[27, 28] For a Hec layer thickness of 0.96 nm, a PEG:Hec volume ratio of 45:55 can be deduced for the crystalline domains. Assuming in a first approximation that the intercalated PEG has the same density than bulk PEG (1.1 g cm^{-3}) and applying the Hec density of 2.7 g cm^{-3}, a filler content of 75 wt% can

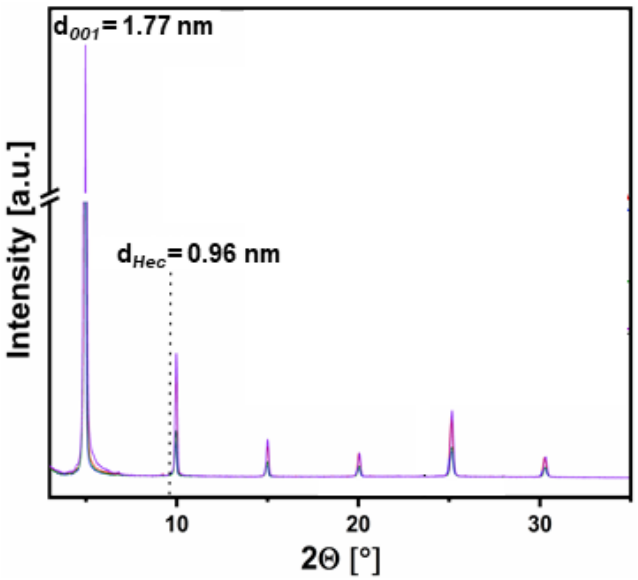

Figure 2. XRD patterns of PEGHec nanocomposites (red: 20wt% filler, blue: 40wt%, green: 60wt%, purple: 75 wt%). The dotted line at 0.96 nm indicates the d-spacing of neat, completely dry Hec (d_{Hec}).

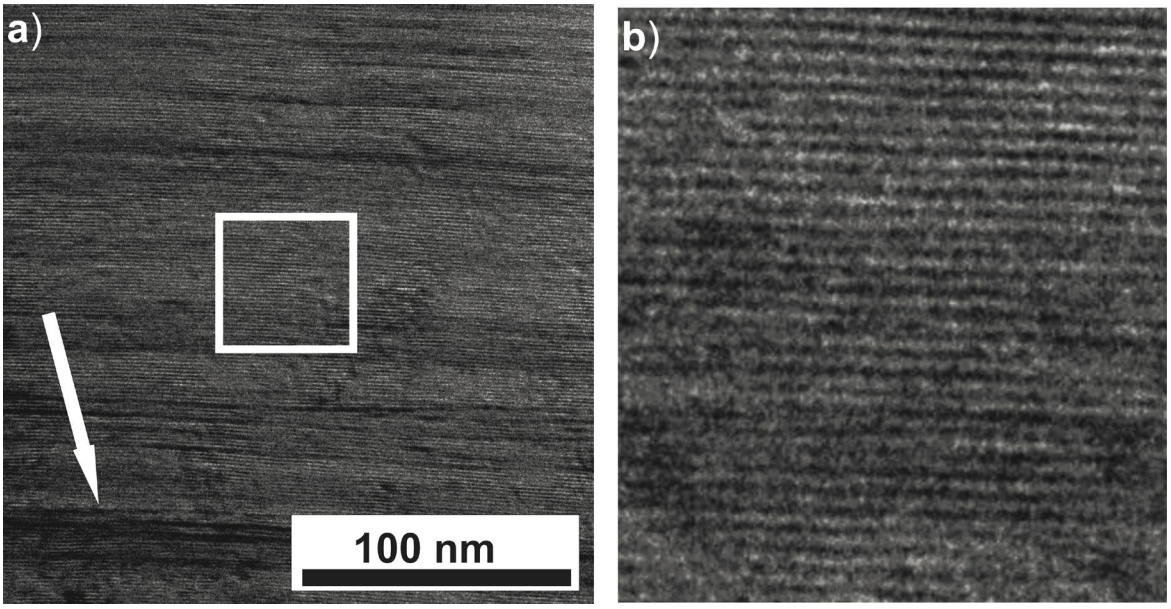

Figure 3. a) TEM image of the highly filled PEGHec nanocomposite (75 wt%) showing extended ordered domains. White arrow indicates partial restacked Hec phase. White inset is shown in b) as close up indicating the equidistant ordering of the Hec nanosheets in the polymer matrix.

be estimated for these crystalline domains. The sample with 75 wt% Hec corresponds to this estimated composition of the crystalline hybrid phase.

TEM images (**Figure 3**a) of this sample showed extended ordered domains. The interlayer height of 0.81 nm (Figure 3b) observed by XRD and TEM agrees with published vaues for PEG layered silicate nanocomposites.[29-31] This 1D ordered intercalated hybrid seems to be a thermodynamically favoured phase irrespective of the type and lateral extension of the layered silicate/clay applied as filler.

A closer inspection of the the TEM images, however, reveals some few layer Hec defects. Apparently, the PEG:Hec ratio applied does not perfectly meet the ratio requested for the hybrid material and consequently some Hec-only domains (Figure 3a, white arrow) are forced to segregate despite thermodynamics favouring the hybrid structure as recently suggested by Walther et al..[32] These Hec domains are, however, far thinner than the coherence length of the X-ray beam and therefore do not show up in the diffraction pattern.

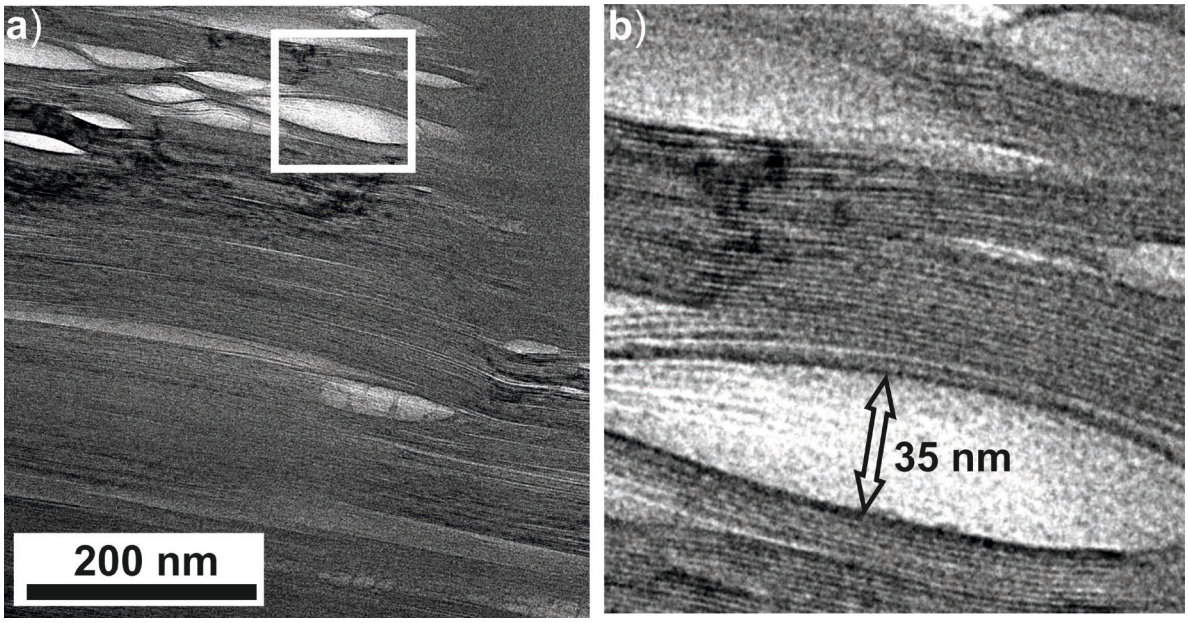

Figure 4. a) TEM image of PEGHec-40 nanocomposite showing neat PEG domains (white box) between the ordered hybrid domains. b) Close up of white box in a) showing the size of the PEG slabs between the hybrid domains matrix.

All other samples prepared being lower in Hec content display the opposite phenomenon. PEG is available in surplus of the stoichiometry of the hybrid phase and consequently needs to segregate in PEG-only domains. As the evaporation progresses, however, a tortuous path is built up in the casted film making mass transport increasingly more difficult and this severely limits the length scale of the segregated domains. Moreover, these domains are inherently 2D and occur as anisotropic eliptical lenses (**Figure 4**a) because the silicate layers with 20 µm lateral extension all orient in parallel in the film. The diffusion limitation defining the kinetics of the mass transport and thus the typical size of the segregated domains, according to Cussler is directly dependant on $\frac{\phi^2}{1-\phi}$ (ϕ= filler content).[25, 33] The slabs of segregated PEG between intercalated hybrid domains therefore become thicker with decreasing Hec content.

For PEGHec-40 typical slab heights in the range of 35 nm are observed (**Figure 4**b). These segregated PEG domains therefore still sense some degree of confinement. Consequently, confinement effects are expected for the segregated PEG

domains since they are far from the bulk state but rather experience a severe confinement between the intercalated domains (**Figure 4**b). The degree of confinement can be systematically varied with the filler content applied. The PEGHec composites thus represent ideal model systems to study the influence of heterogeneous nucleation surface and confinement on the crystallization behavior of PEG.

These structural results are in line with the non-isothermal DSC scans performed in this work reported in **Figure 5**. As can be seen in the DSC scans, the addition of Hec increases the peak crystallization temperature. The results are consistent with a nucleating effect that is maximum for 20 wt% filler content (as T_c is the highest) and progressively reduces, as the amount of Hec is increased. The peak crystallization temperature (T_c) increases from 22 °C to 34 °C upon 20 wt% Hec addition (Figure 5). With further increases in the amount of Hec (40, 60 and 75 wt%)

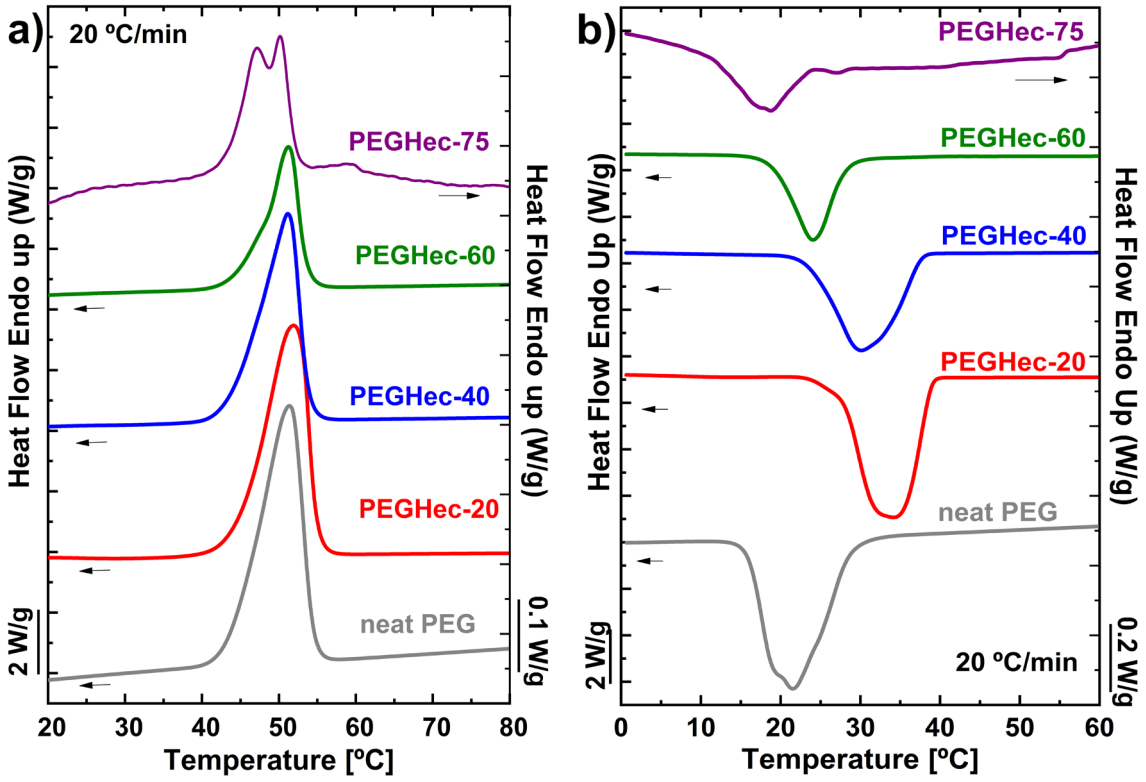

Figure 5. DSC scans (a,b) of the different nanocomposites (red: 20wt% filler, blue: 40wt%, green: 60wt%, purple: 75 wt%) in comparison with neat PEG (grey).

confinement increases. A competition occurs between the nucleating effect of Hec (which tends to increase T_c) and its confinement effect on PEG (which tends to decrease T_c). The 1D-crystalline intercalation compound obtained at 75 wt% Hec, even shows a T_c of 19°C that is below the T_c of neat PEG (22°C) and an extremely low crystallinity degree (see **Figure 5**b). This indicates that strong confinement is the dominant behavior. This verification is in agreement with recent results obtained by Walther et al. and published in Reference 32, where they confirmed the presence of a crystalline phase of PEO in all nanocomposite samples.

Figure 6 summarizes the non-isothermal DSC results by plotting T_c, T_m, and the degree of crystallinity (X_c) versus Hec content in the composites (see **Table S1**). As can be clearly seen, the crystallinity of the PEGHec composites strongly decreases with an increasing amount of Hec. This effect leads to a crystallinity of < 5% in PEGHec-75. As already disussed, the space for segregated PEG-only domains

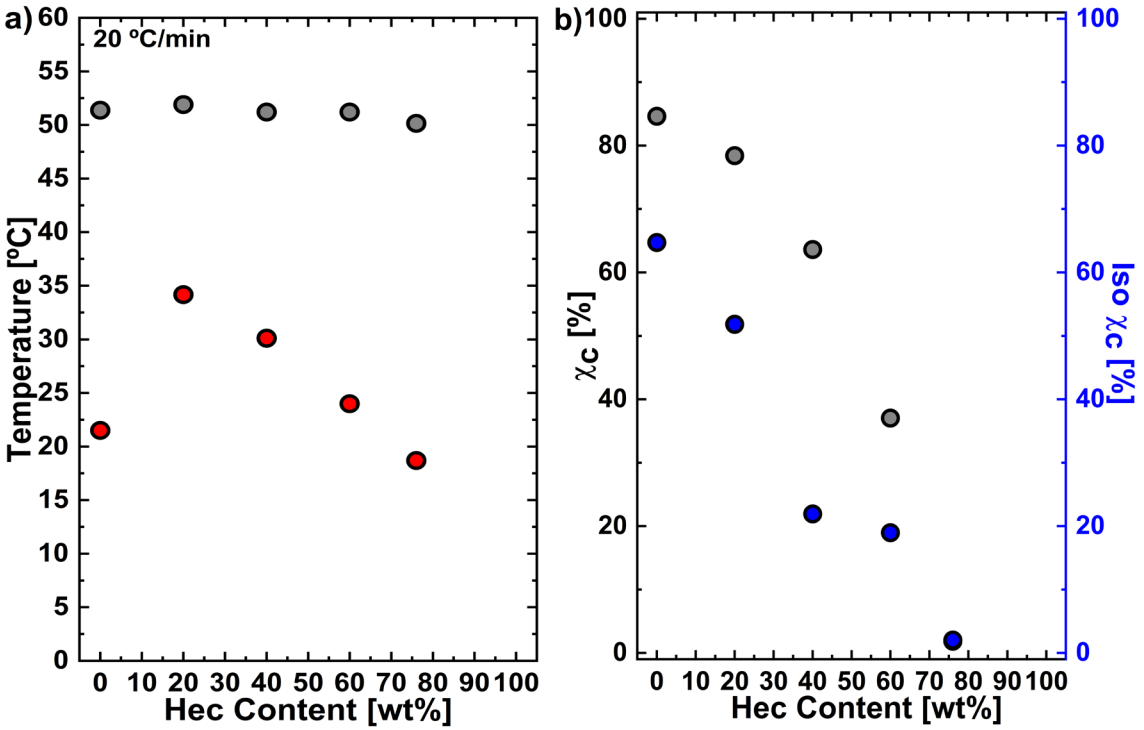

Figure 6. a) Experimental melting temperatures (grey circles) and crystallization temperatures (red cicles); b) calculated degree of crystallinity developed during non-isothermal crystallization (grey circles) and during isothermal crystallization (blue circles) determined as a function of the Hec content in the composites.

between the perfectly ordered hybrid phase is affected by the amount of Hec, which significantly hinders PEG to crystallize. Within the confined space PEG is not able to crystallize and the crystallinity is given by the separated PEG phase outside the galleries of Hec. Compared to other publications in the field of polymer-filler crystallinity studies, we observed a large decrease of crystallinity with increasing filler content (Figure 6b) up to very high loadings.[34] The hybrid materials even keep a significant crystallinity at filler contents as high as 60 wt%.[34]

By polarized light optical microscopy (PLOM, **Figure 7**) the nucleating effect of Hec can be observed. For neat PEG, the isothermal growth of negative spherulites at 40 ºC was easily observed, as PEG develops large spherulites with diameters of around 400 μm (see Figure 7a). In the case of the sample with 20% Hec, the birefringent colors observed in Figure 7b and 7c are due to Hec nanosheets that are viewed edge-on. Figure 7c shows that birefringent crystals nucleate directly around the areas where the Hec nanosheets are located. They are acting as nuclei for the surrounding PEG matrix crystallisation. From these starting points, PEG chains nucleate and PEG crystal aggregates (resembling irregular axialites) grow impinging on one another.

To calculate the efficiency of Hec as a nucleating agent for PEG we employ the self nucleation (SN) technique. (**Figure 8**, **Table 1**) Müller et al. have applied SN

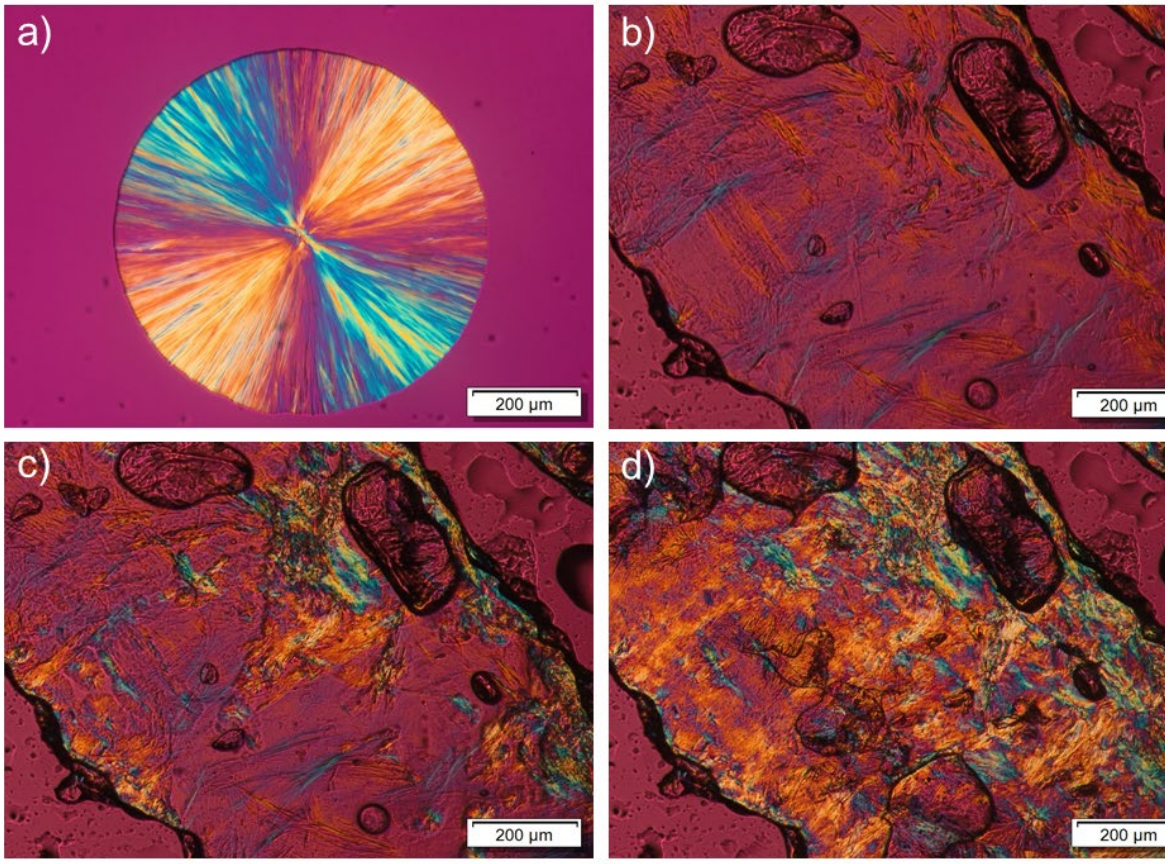

Figure 7. PLOM micrographs of a) a single PEG spherulite crystallized isothermally at 40 ºC and the time-dependant crystallization of PEGHec-20 sample crystallized at 40 ºC at b) t= 0 seconds, c) t= 20 seconds, d) t= 60 seconds.

protocols to study the confined crystallization in copolymers and nanocomposites/hybrids, among other polymeric systems.[19, 20, 35] The protocol used here is detailed in the experimental section.

Figure 8a presents the cooling scans after SN at the indicated T_s values. Figure 8b shows the subsequent heating scans from the same T_s values. With the cooling DSC scans of Figure 8a, the transition between *Domain I* and *II* can be clearly established, while the transition between *Domains II* and *III* can be detected by analyzing the heating DSC scans of Figure 8b. *Domain I* or melting domain (red lines) in Figure 8 occurs at T_s temperatures where all crystalline memory is erased. This *Domain* is characterized by a constant T_c as is observed in Figure 6a and invariant T_m value as is observed in Figure 8b.

Domain I switches to *Domain II* when the T_c increases to higher temperatures (as T_s is lowered). This *Domain* is also called the *exclusive self-nucleation domain*. In *Domain II* the T_s values are low enough to induce the formation of self-nuclei but high enough to guarantee that annealing does not occur. *Domain II* can be observed in Figure 8a (DSC scans are plotted with blue lines) and is first detected when T_c values increase in comparison with the standard T_c value observed in *Domain I*. The lowest T_s value within *Domain II* identifies the "ideal self-nucleation temperature" ($T_{s,ideal}$), a temperature that should be carefully measured. The ideal self-nucleation temperature is the Ts temperature that provokes maximum self-nucleation (i.e., maximum increase in the concentration of self-nucleai within Domain II) but without producing annealing. According to Figure 8a, the ideal SN temperature for the employed PEG in this work is 48 ºC. If the applied temperature gets too low, melting is incomplete and annealing sets in. This is characteristic for *Domain III* where a second melting peak appear, as it can be observed in Figure 8b (DSC plotted with green lines).

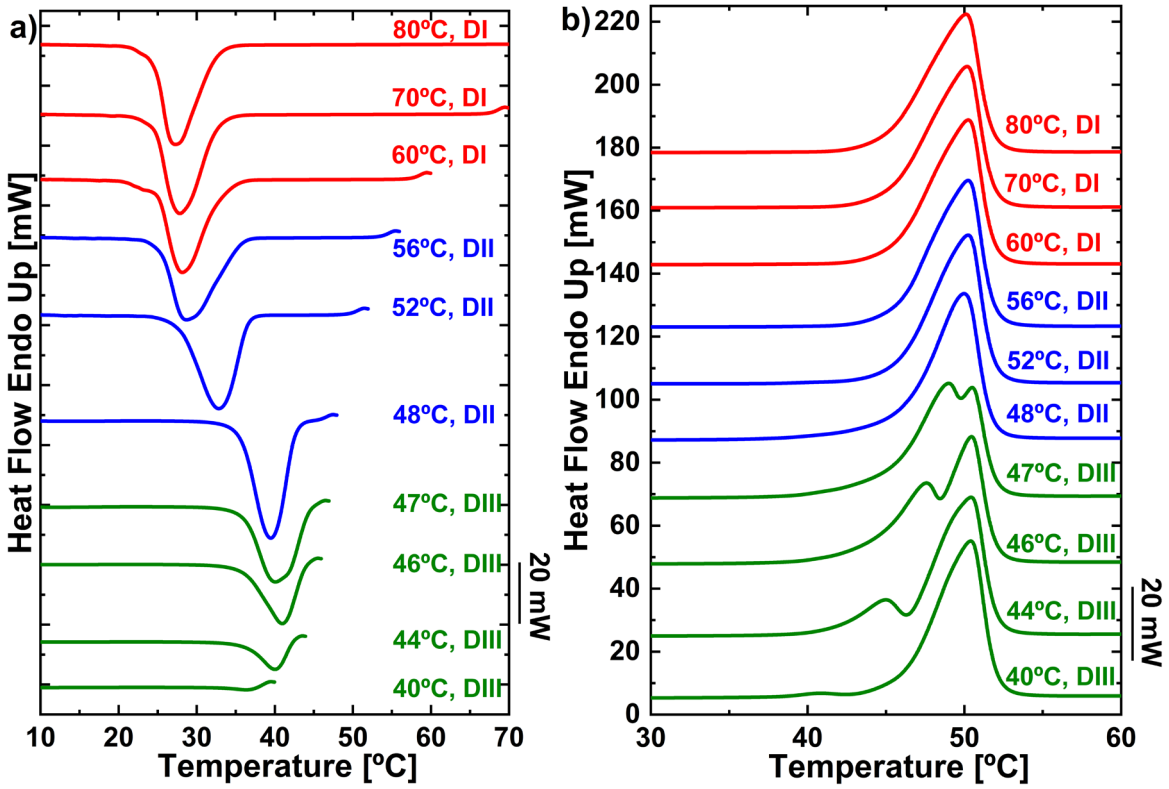

Figure 8. Cooling (a) and heating (b) scans for neat PEG after SN at different T_s values and presented from top to bottom in decreasing T_s order *Domain I* (red), *II* (blue), *III* (green) are shown.

According to Fillon et al. the nucleation efficiency (NE) of a nucleating agent can be easily calculated by using the information obtained by SN measurements.[36] As explained above, self-nuclei are the most efficient nuclei for polymer crystallisation and thereby, the lowest applied temperature in *Domain II* is expected to be the most efficient temperature for SN ($T_{s,ideal}$), as with decreasing temperature, the nuclei number is increasing. Thereby, the T_c value after SN at 48 °C (i.e., the ideal SN temperature for the PEG employed here, as shown in Figure 8) or $T_{c,max}$ is taken for the calculation of the different NEs (**Equation (1)**).

$$NE = \frac{T_{c,NA} - T_{c,P}}{T_{c,max} - T_{c,P}} \cdot 100 \quad (1)$$

where $T_{c,NA} = T_c$ (PEGHec-X) and $T_{c,P} = T_c$ (neat PEG) = 22°C, taken from Figure 5. (For neat PEG, Figure 8, $T_{c,max}$ = 40 °C)

The calculated nucleation efficiencies are reported in Table 1. At 20% Hec, a realtively high nucleation efficiency of 67% is obtained. However, as Hec content

increases, the efficiency of Hec as a nucleating agent is offset by its confinement effect and the calculated efficiency decreases dramatically, until it vanishes at very large Hec contents.

Table 1. Nucleation efficiencies calculated from Equation 1 (see text).

Sample	T_c / °C	NE / %
PEGHec-20	34	67
PEGHec-40	30	45
PEGHec-60	25	17
PEGHec-75	19	0

Additionally, calorimetry experiments were used to measure the overall isothermal crystallization rate of neat PEG and the PEGHec composites. A polymer overall crystallization rate depends on both primary nucleation rate and crystal growth rate. The experimentally measured half-crystallization time ($1/\tau_{1/2}$) is proportional to the overall crystallization rate. The half-crystallisation time is defined as the time needed for 50% relative conversion from the melt to the crystalline state.

Figure 9a shows the overall crystallization rates (expressed as $1/\tau_{1/2}$) for neat PEG and all PEGHec composites as a function of T_c. The curves show the expected trend of reduction of overall rate as a function of T_c usually observed at low supercoolings, where the crystallization kinetics is dominated by nucleation effects (i.e., primary and secondary nucleation) and much less affected by diffusion.[37]

When 20 wt% Hec is added to PEG, the curve of rate versus T_c in Figure 9a is shifted to higher crystallization temperatures or lower supercoolings. This is a clear acceleration effect of the overall crystallization kinetics provoked by the primary heterogeneous nucleation effect of Hec (which in non-isothermal conditions has a 67%

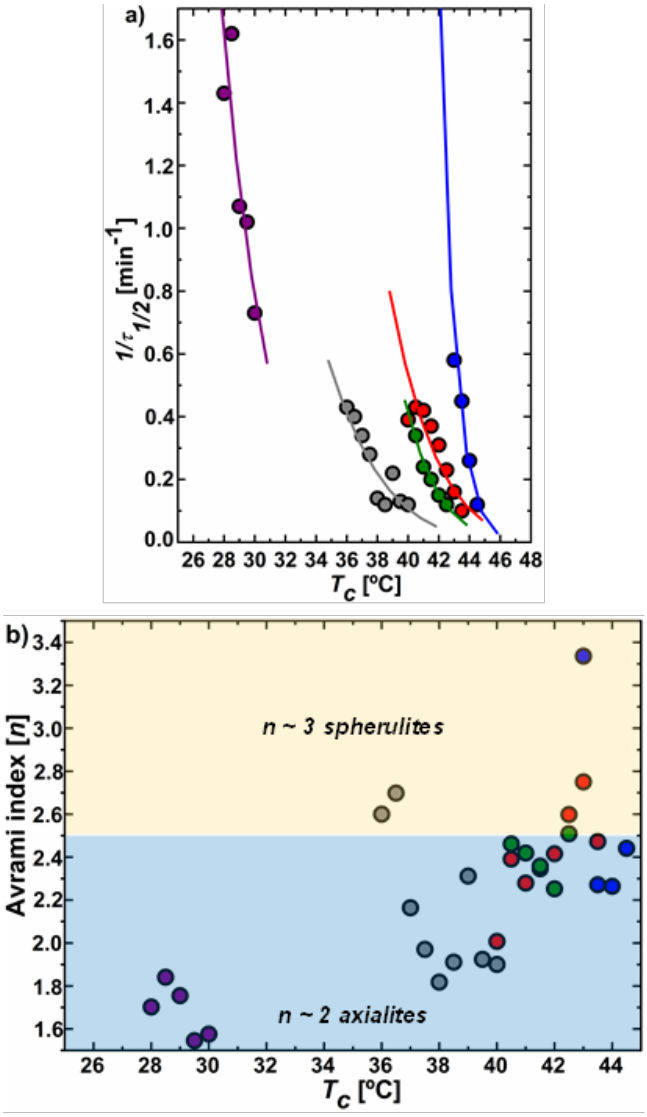

Figure 9. (a) Inverse of the half-crystallization time ($1/\tau_{1/2}$) as a function of T_c and (b) Avrami index (n) as a function of T_c. (red:20wt% filler, blue: 40wt%, green: 60wt%, purple: 75 wt%, grey: neat PEG)

nucleation efficiency, see Table 1) on PEG. Increasing the amount of Hec to 40 wt%, increases even further the overall crystallization kinetics. This indicates that primary nucleation is still controlling the overall crystallization kinetics. However, when 60 wt% Hec is added to PEG, confinement effects start to be present. Hec can still nucleate PEG, but Figure 9a shows that 60 wt% filler content accelerates the overall kinetics less than adding 40 wt% Hec.

Finally, when the amount of Hec increases to 75 wt%, Figure 9a shows how the overall crystallization rate versus T_c curve is shifted to higher supercoolings with

respect to PEG, i.e., a slower kinetics is promoted in relative terms if constant crystallization temperatures are considered (by extrapolation). This result means that confinement effects completely dominate the overall crystallization kinetics and the primary nucleation effect of Hec is less important.

Generally speaking, if we extrapolate all data to a single crystallization temperature in Figure 9a, the results show that Hec addition increases overall crystallization rate until a maximum is obtained at 40 wt%, then further Hec addition decreases the crystallization rate. The isothermal crystallization kinetics shows remarkable trends that are consistent with an acceleration effect due to primary nucleation enhancement at low hectorite contents and at higher filler loadings, a reduction due to confinement of PEG chains by the filler.

The competition between primary nucleation and confinement in the overall crystallization kinetics results shown in Figure 9a is very clear. In the last few years similar trends have been reported for similarly confined materials, containing carbon nanotubes and silica nanoparticles, amongst others.[4, 13, 14, 38]

The overall crystallization kinetics data can be modeled by the Avrami equation, even if the fittings to the Avrami equation are usually restricted to low conversions to the crystalline state, i.e., the primary crystallization stage (before crystalline superstructural aggregates impinged on one another during growth).[18, 39]

Thereby, the Avrami index (n) (Figure 9b) provides a useful tool to have a deeper look into the crystallization kinetics with respect to the morphology. As proposed by Müller et al. [38, 40, 41] the Avrami index can be considered the sum of two parts (**Equation (2)**):

$$n = n_n + n_{gd} \qquad (2)$$

where n_n describes the fraction of the index related to primary nucleation (n_n=0 instantaneous nucleation and n_n=1 sporadic nucleation). The value n_{gd} shows the growth dimensionality (usually 1−3, n_{gd} = 1 (one-dimensional crystals), n_{gd} = 2 (axialites, 2D) and n_{gd} = 3 (spherulites, 3D)).

Figure 9b shows how the Avrami index varies with crystallization temperature. At low filler contents, the nucleating effect leads to the formation of instantaneously nucleated spherulites or axialites, for which an Avrami index of 3 and 2 respectively should be expected. Within experimental errors and the fact that nucleation is normally not perfectly instantaneous, fractional values of the Avrami index are usually obtained. In samples with a Hec content between 20 and 60 wt%, the Avrami values are around 2.2-2.7. On the other hand, when the Hec content increased to 75 wt%, the Avrami index decreased drastically to values around 1.6-1.8, due to the increasing confinement effect due to Hec. An Avrami index value of 2 would be expected for 2D crystal aggregates instantaneously nucleated, or 1D crystals sporadically nucleated. As it has been observed in literature before in similar nanocomposites/hybrids,[13, 14] a close correlation exists between Avrami index and confinement. Additionally, as confinement increases the composites need higher degrees of supercooling to crystallize.

As confinement increases, the slow step of the kinetics becomes the nucleation, as growth is usually very fast at high supercoolings and the small spaces where the material crystallizes can be quickly filled by crystal growth, once one nucleous is formed. This is the rationale behind the close correlation between decreases in Avrami index and confinement.[38-41]

The Lauritzen and Hoffman (LH) model can be used to fit the isothermal overall crystallization rate data. Further insights into the nucleation versus confinement

competition can be gathered from the interpretation of the fitting parameters.[42-44] The LH model applied to DSC data (including both nucleation and growth) is expressed by **Equation (3)**:

$$\frac{1}{T_{0.5}}(T) = \frac{1}{T_{0.5}}(T=0)\exp\left(\frac{-U^*}{R(T_c-T_\infty)}\right)\exp\left(\frac{-K_g^T}{\Delta T f\, T_c}\right) \qquad (3)$$

$1/\tau_{0.5}$ represents the overall crystallisation rate (nucleation+growth, obtained from DSC).

U^* is a diffusion activation energy (taken as 1500 cal/mol)

R is the gas constant.

T_c is the isothermal crystallization temperature.

T_∞ is a temperature where chain mobility stops (taken as T_g - 30 K).

ΔT defines the supercooling (T_m^0-T_c), and T_m^0 is the equilibrium melting temperature.

f is defined as: $f=\frac{2T_c}{(T_c+T_m^0)}$

Table 2. Fitting parameters of the LH theory applied to the overall isothermal crystallization data measured by DSC.

samples	K_g x 10^4 (K^2)	σ_e (erg/cm^2)	q x 10^{-13} (erg)	R^2
neat PEG	4.3	41.3	1.79	0.7826
PEGHec-20	3.1	30.4	1.32	0.8969
PEGHec-40	2.6	25.5	1.11	0.9753
PEGHec-60	3.5	34.2	1.48	0.9875
PEGHec-75	5.2	51.5	2.24	0.8804

Values employed for the L-H fitting: ρc =1.239 g/cm^3; ρa=1.124 g/cm^3 Å[45]
T_∞=-97.2 ºC; a_0=4.67 Å b_o=4.65 Å; U^*= 1500 Cal/mol; Δh_f = 230 J/g[46]

The value K_g^T is given by the slope of the graph $\ln\frac{1}{T_{0.5}} + \frac{U^*}{R(T_c-T_\infty)}$ against $(\Delta T f\, T_c)^{-1}$. K_g^T is proportional to the energy barrier of the overall crystallization. **Table 2** shows all relevant parameters that can be obtained by the fitting of the LH model .[47]

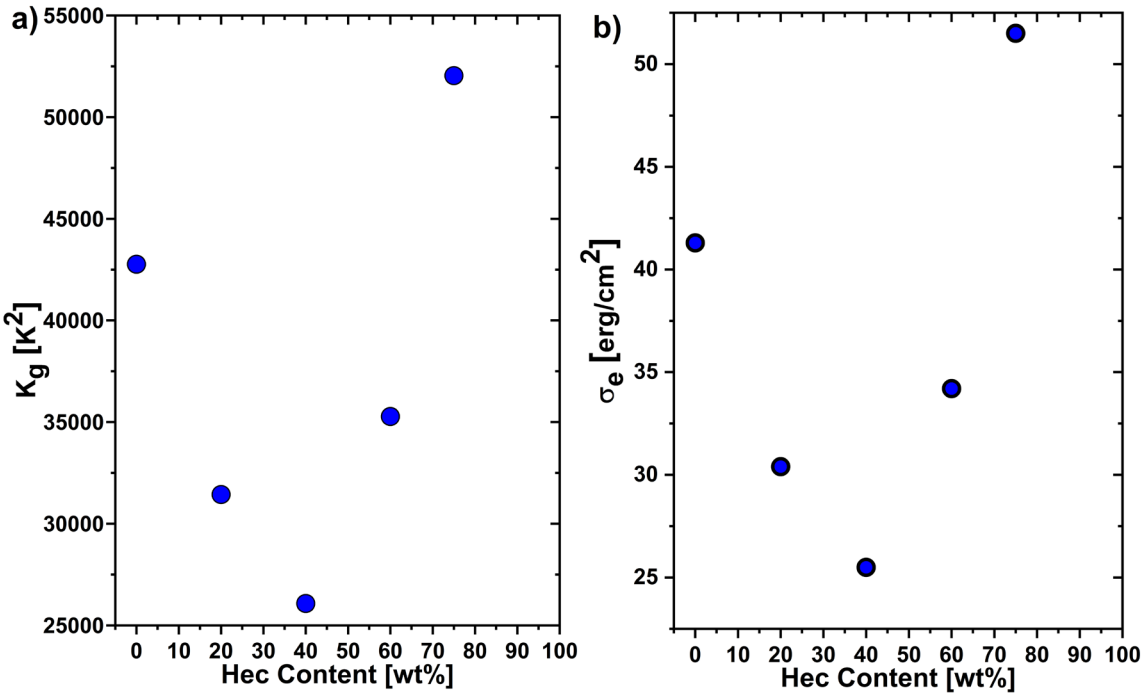

Figure 10. K_g (a)) and σ (b)) versus Hec Content.

As shown **in Figure 10** and Table 2, the energy barrier for overall crystallization (proportional to K_g^T), the fold surface free energy σ_e and the work of chain folding q, decrease first with increasing Hec content, passing thorugh a minimum at 40 wt% Hec, as expected in view of the nucleating effect of Hec. A similar effect has also already been observed and examined with the LH theory for PE layered silicate nanocomposites.[48] With further increases of filler loading, the described values increase again and the energy barrier ends up being higher than that for neat PEG at a Hec content of 75 wt%. Ghasemi et al.[48] described an increased surface energy and work of chain folding as hindered re-entry of the polymer chains into the crystal due to the Hec nanosheets. The results presented in Figure 10 provide additional evidences of the nucleation versus confinement competition that occurs upon Hec addition to PEG.

4. Conclusions

Due to the large diameter (20 µm) of individual silicate layers upon repulsive delamination, liquid crystalline phases are obtained with separations of neighbouring nanosheets of > 40 nm. This allows the formation of a homogenous nematic ternary dispersion (water, PEG, Hec). Upon removing the dispersion medium, thermodynamics drives a partial phase segregation. Since mass transport is hindered during the drying process, kinetics of segregation are slowed down and the length scale at which phase segregation can be accomplished varies systematically with filler content.

A clear competition between heterogeneous nucleation and confinement imposed on PEG by increasing amounts of Hec has been demonstrated by changes in thermal properties, isothermal crystallization kinetics of PEG as a function of filler content, Avrami index trends and crystallization energy barrier variations.

Aside of the more fundamental aspects, the PEGHec composites with their tailor-made crystallinity and a very long tortuous path for gas molecules, may have potential as biodegradable barrier systems, particularily of interest as food packaging material. Work in that direction is in progress.

Acknowledgements

The authors thank Florian Puchtler for producing the synthetic sodium hectorite, Marco Schwarzmann for the SEM and TEM measurements and sample preparation via cryo ion slicing, and Dr. Sabine Rosenfeldt for the SAXS measurements. We appreciate the support of the Keylab for Optical and Electron Microscopy and the Keylab for Small Scale Polymer Processing of the Bavarian Polymer Institute (BPI). This work was supported by the German Science Foundation (DFG) within the

collaborative research project SFB 1357. J.M. acknowledges support from the Provincial Council of Gipuzkoa under the program Fellow Gipuzkoa and partial financial support to the IBERDROLA Foundation. J.L.O.M. wish to thank the National Council of Science and Technology (CONACYT) in México for his grant 471837. We acknowledge funding by Mineco MAT2017-83014-C2-1-P project and by the Basque Government through grant IT1309-19. This work has also received funding from the European Union´s Horizon 2020 research and innovation program under the Marie Sklodowska-Curie grant agreement No 778092.

Appendix A. Supporting information

Supporting Information is available from the Online Library or from the author.

References

1. Popescu, M.-C.; Dogaru, B.-I.; Sun, D.; Stoleru, E.; Simionescu, B., Structural and sorption properties of bio-nanocomposite films based on κ-carrageenan and cellulose nanocrystals. *Int. J. Biol. Macromol* **2019,** *135*, 462-471.
2. Nalwa, H. S., *Handbook of nanostructured materials and nanotechnology, five-volume set*. Academic Press: 1999.
3. Ajayan, P. M.; Zhou, O. Z., Applications of carbon nanotubes. In *Carbon nanotubes*, Springer: Berlin, Heidelberg, 2001; pp 391-425.
4. Michell, R. M.; Müller, A. J., Confined crystallization of polymeric materials. *Prog. Polym. Sci.* **2016,** *54*, 183-213.
5. Frensch, H.; Harnischfeger, P.; Jungnickel, B.-J., Fractionated crystallization in incompatible polymer blends. In *Multiphase Polymers: Blends and Ionomers*, ACS Publications: 1989; pp 101-125.
6. Arias-Trujillo, J.; Matías-Sanchez, A.; Cantero, B.; López-Querol, S., Effect of polymer emulsion on the bearing capacity of aeolian sand under extreme confinement conditions. *Constr. Build. Mater.* **2020,** *236*, 117473.
7. Cavallaro, G.; De Lisi, R.; Lazzara, G.; Milioto, S., Polyethylene glycol/clay nanotubes composites. *J. Therm. Anal. Calorim.* **2013,** *112*, 383-389.
8. Hutanu, D.; Frishberg, M. D.; Guo, L.; Darie, C. C., Recent applications of polyethylene glycols (PEGs) and PEG derivatives. *Mod. Chem. Appl.* **2014,** *2*, 1-6.
9. Ghyati, S.; Benhamou, M.; El-Jai, M.; Akhrif, I., Polymer nanocomposites from natural clay: Understanding clay-PEG interaction and their effect on spacing between clay-plates. *OAJ Materials and Devices* **2018,** *3*, 1103.
10. Liu, Y.; Meng, H.; Konst, S.; Sarmiento, R.; Rajachar, R.; Lee, B., Injectable Dopamine-Modified Poly(ethylene glycol) Nanocomposite Hydrogel with Enhanced Adhesive Property and Bioactivity. *ACS Appl. Mater. Interfaces.* **2014,** *6*, 16982–16992.
11. Papananou, H.; Perivolari, E.; Chrissopoulou, K.; Anastasiadis, S. H., Tuning polymer crystallinity via the appropriate selection of inorganic nanoadditives. *Polymer* **2018,** *157*, 111-121.

12. Zhu, L.; Mimnaugh, B. R.; Ge, Q.; Quirk, R. P.; Cheng, S. Z.; Thomas, E. L.; Lotz, B.; Hsiao, B. S.; Yeh, F.; Liu, L., Hard and soft confinement effects on polymer crystallization in microphase separated cylinder-forming PEO-b-PS/PS blends. *Polymer* **2001,** *42*, 9121-9131.
13. Müller, A. J.; Arnal, M. L.; Trujillo, M.; Lorenzo, A. T., Super-nucleation in nanocomposites and confinement effects on the crystallizable components within block copolymers, miktoarm star copolymers and nanocomposites. *Eur. Polym. J.* **2011,** *47*, 614-629.
14. Wen, X.; Su, Y.; Shui, Y.; Zhao, W.; Müller, A. J.; Wang, D., Correlation between grafting density and confined crystallization behavior of poly (ethylene glycol) grafted to silica. *Macromolecules* **2019,** *52*, 1505-1516.
15. Kawai, F., Microbial degradation of polyethers. *Appl. Microbiol. Biotechnol.* **2002,** *58*, 30-38.
16. Kalo, H.; Möller, M. W.; Ziadeh, M.; Dolejš, D.; Breu, J., Large scale melt synthesis in an open crucible of Na-fluorohectorite with superb charge homogeneity and particle size. *Appl. Clay Sci.* **2010,** *48*, 39-45.
17. Kalo, H.; Möller, M. W.; Kunz, D. A.; Breu, J., How to maximize the aspect ratio of clay nanoplatelets. *Nanoscale* **2012,** *4*, 5633-5639.
18. Lorenzo, A. T.; Arnal, M. L.; Albuerne, J.; Müller, A. J., DSC isothermal polymer crystallization kinetics measurements and the use of the Avrami equation to fit the data: Guidelines to avoid common problems. *Polym. Test.* **2007,** *26*, 222-231.
19. Fillon, B.; Wittmann, J.; Lotz, B.; Thierry, A., Self-nucleation and recrystallization of isotactic polypropylene (α phase) investigated by differential scanning calorimetry. *J. Polym. Sci. Pol. Phys.* **1993,** *31*, 1383-1393.
20. Müller, A. J.; Arnal, M. L., Thermal fractionation of polymers. *Prog. Polym. Sci.* **2005,** *30*, 559-603.
21. Tsurko, E. S.; Feicht, P.; Habel, C.; Schilling, T.; Daab, M.; Rosenfeldt, S.; Breu, J., Can high oxygen and water vapor barrier nanocomposite coatings be obtained with a waterborne formulation? *J. Membr. Sci.* **2017,** *540*, 212-218.
22. Tsurko, E. S.; Feicht, P.; Nehm, F.; Ament, K.; Rosenfeldt, S.; Pietsch, I.; Roschmann, K.; Kalo, H.; Breu, J., Large Scale Self-Assembly of Smectic Nanocomposite Films by Doctor Blading versus Spray Coating: Impact of Crystal Quality on Barrier Properties. *Macromolecules* **2017,** *50*, 4344-4350.
23. Doblhofer, E.; Schmid, J.; Rieß, M.; Daab, M.; Suntinger, M.; Habel, C.; Bargel, H.; Hugenschmidt, C.; Rosenfeldt, S.; Breu, J., Structural Insights into Water-Based Spider Silk Protein–Nanoclay Composites with Excellent Gas and Water Vapor Barrier Properties. *ACS Appl. Mater. Interfaces* **2016,** *8*, 25535-25543.
24. Stöter, M.; Kunz, D. A.; Schmidt, M.; Hirsemann, D.; Kalo, H.; Putz, B.; Senker, J.; Breu, J., Nanoplatelets of Sodium Hectorite Showing Aspect Ratios of≈ 20 000 and Superior Purity. *Langmuir* **2013,** *29*, 1280-1285.
25. Kunz, D. A.; Schmid, J.; Feicht, P.; Erath, J.; Fery, A.; Breu, J., Clay-based nanocomposite coating for flexible optoelectronics applying commercial polymers. *ACS nano* **2013,** *7*, 4275-4280.
26. Rosenfeldt, S.; Stöter, M.; Schlenk, M.; Martin, T.; Albuquerque, R. Q.; Förster, S.; Breu, J., In-Depth Insights into the Key Steps of Delamination of Charged 2D Nanomaterials. *Langmuir* **2016,** *32*, 10582-10588.
27. Moore, D. M.; Reynolds, R. C., *X-ray Diffraction and the Identification and Analysis of Clay Minerals*. Oxford university press Oxford: 1989; Vol. 322.
28. Bailey, S. W., Nomenclature for regular interstratifications. *Am. Mineral.* **1982,** *67*, 394-398.
29. Aranda, P.; Ruiz-Hitzky, E., Poly (ethylene oxide)-silicate intercalation materials. *J. Mater. Chem.* **1992,** *4*, 1395-1403.
30. Wu, J.; Lerner, M. M., Structural, thermal, and electrical characterization of layered nanocomposites derived from sodium-montmorillonite and polyethers. *J. Mater. Chem.* **1993,** *5*, 835-838.

31. Chaiko, D. J., New Poly (ethylene oxide)− Clay Composites. *Chem. Mater.* **2003,** *15*, 1105-1110.
32. Eckert, A.; Abbasi, M.; Mang, T.; Saalwächter, K.; Walther, A., Structure, Mechanical Properties, and Dynamics of Polyethylenoxide/Nanoclay Nacre-Mimetic Nanocomposites. *Macromolecules* **2020,** *53*, 1716-1725.
33. Choudalakis, G.; Gotsis, A., Permeability of polymer/clay nanocomposites: a review. *Eur. Polym. J.* **2009,** *45*, 967-984.
34. Chrissopoulou, K.; Andrikopoulos, K.; Fotiadou, S.; Bollas, S.; Karageorgaki, C.; Christofilos, D.; Voyiatzis, G.; Anastasiadis, S., Crystallinity and chain conformation in PEO/layered silicate nanocomposites. *Macromolecules* **2011,** *44*, 9710-9722.
35. Michell, R.; Mugica, A.; Zubitur, M.; Müller, A. J., Self-nucleation of crystalline phases within homopolymers, polymer blends, copolymers, and nanocomposites. In *Polymer Crystallization I*, Springer: 2015; pp 215-256.
36. Fillon, B.; Lotz, B.; Thierry, A.; Wittmann, J., Self-nucleation and enhanced nucleation of polymers. Definition of a convenient calorimetric “efficiency scale” and evaluation of nucleating additives in isotactic polypropylene (α phase). *J. Polym. Sci. Pol. Phys.* **1993,** *31*, 1395-1405.
37. Mandelkern, L., *Crystallization of Polymers: Volume 2, Kinetics and Mechanisms*. Cambridge University Press: 2004.
38. Michell, R. M.; Blaszczyk-Lezak, I.; Mijangos, C.; Müller, A. J., Confinement effects on polymer crystallization: From droplets to alumina nanopores. *Polymer* **2013,** *54*, 4059-4077.
39. Müller, A. J.; Michell, R. M.; Lorenzo, A. T., Isothermal crystallization kinetics of polymers. *Polymer Morphology: Principles, Characterization, Processing* **2016**, 181-203.
40. Müller, A. J.; Balsamo, V.; Arnal, M. L., Nucleation and crystallization in diblock and triblock copolymers. In *Block Copolymers II*, Springer: 2005; pp 1-63.
41. Michell, R. M.; Müller, A. J., Confined crystallization of polymeric materials. *Prog. Polym. Sci.* **2016,** *54*, 183-213.
42. Lorenzo, A. T.; Müller, A. J.; Lin, M.-C.; Chen, H.-L.; Jeng, U.-S.; Priftis, D.; Pitsikalis, M.; Hadjichristidis, N., Influence of macromolecular architecture on the crystallization of (PCL2)-b-(PS2) 4-miktoarm star block copolymers in comparison to linear PCL-b-PS diblock copolymer analogues. *Macromolecules* **2009,** *42*, 8353-8364.
43. Trujillo, M.; Arnal, M. L.; Müller, A. J.; Mujica, M. A.; de Navarro, C. U.; Ruelle, B.; Dubois, P., Supernucleation and crystallization regime change provoked by MWNT addition to poly (ε-caprolactone). *Polymer* **2012,** *53*, 832-841.
44. Guo, Q., *Polymer morphology: principles, characterization, and processing*. John Wiley & Sons: 2016.
45. Brandrup, J.; Immergut, E.; Grulke, E., *Polymer Handbook*. John Wiley & Sons Inc: New York, 1999.
46. Mark, J. E., Polymer Data Handbook. *Oxford University Press* **1999**.
47. Castillo, R. V.; Müller, A. J., Crystallization and morphology of biodegradable or biostable single and double crystalline block copolymers. *Prog. Polym. Sci.* **2009,** *34*, 516-560.
48. Ghasemi, H.; Carreau, P. J.; Kamal, M. R., Isothermal and non-isothermal crystallization behavior of PET nanocomposites. *Polym. Eng. Sci.* **2012,** *52*, 372-384.

Table of Contents

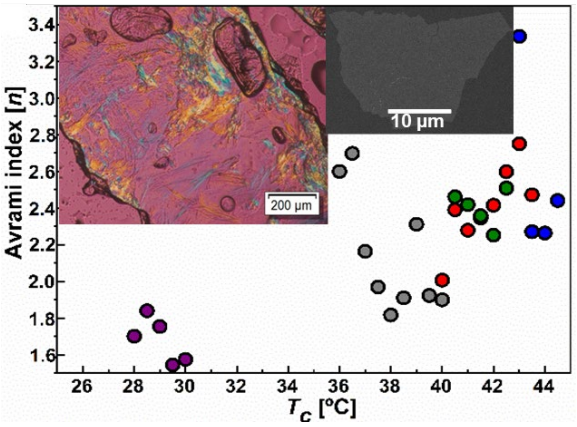

The influence of a high aspect ratio layered silicate onto the crystallization kinetics of polyethylene glycol (PEG) was investigated. Systematic variation of the filler content allows tuning the nanocomposite structure and in this way study the competition of nucleation and confinement.

Competition between nucleation and confinement in the crystallization of poly(ethylene glycol)/large aspect ratio hectorite composites

Christoph Habel[1,†] Jon Maiz[2,†], Jorge L. Olmedo-Martínez[2], Juan V. López[3], Josef Breu[1], Alejandro J. Müller[2,4*]*